Entanglement properties of an ultracold atom interacting with a cavity quantized electromagnetic field

L. O. Castaños and R. Jáuregui

Instituto de Física, Universidad Nacional Autónoma de México, Apdo. Postal 20-364, México 01000, México
(Received 2 July 2010; published 15 November 2010)

We study the temporal evolution of the properties of a two-level atom coupled to a single-mode cavity field without dissipation with its center-of-mass motion quantized in one dimension. It is shown that, starting with a separable state, genuine tripartite entangled states can be generated under resonance conditions of the light frequency and atom transition frequency in the cold regime. The onset of Rabi oscillations is analyzed and explicit predictions for properties like emission probability and dispersions for the center-of-mass position and momenta are given for resonance and detuned conditions. Transmission-resonance effects on entanglement and other properties are also analyzed. Comparisons with the semiclassical adiabatic approximation predictions are also made.

I. INTRODUCTION

The advent of laser-cooling techniques and experiments involving cavity quantum electrodynamics (CQED) gave rise to a growing interest to explore the dynamics of cold atoms interacting with quantized cavity fields [1–14]. A paradigmatic model used to study this coupled dynamics is that of a two-level atom with its center-of-mass (c.m.) motion quantized in one dimension (normally taken to be the z direction) interacting with a single-mode cavity field. Although in most current experiments with single atoms the center of mass does not need to be treated quantum mechanically [7], using this model it has been theoretically recognized that the atom dipole-electromagnetic field coupling opens the possibility of dramatic consequences [1–6]: Sufficiently cold atoms may be reflected by the cavity field and the induced emission process would be intimately associated with the atom center-of-mass motion. To distinguish this process from the usual stimulated emission, the concept of microwave amplification via z-motion-induced emission of radiation (mazer) was introduced [3]. Furthermore, in Ref. [4] a lossy cavity pumped by cold atoms was considered, and the Born-Markov secular master equation for the cavity field was obtained. Using this, it was found that the photon distribution differs completely from that of a cavity pumped by thermal atoms. Also, it was shown that the mazer properties depend greatly on the cavity mode profile. Results were presented for the mesa function, sech^2 function, and sinusoidal modes [5]. More recently, Ref. [8] considered the stationary states of a nonresonant interaction and the mesa function mode to show that the cavity field could slow down or speed up the atoms and block the emission process according to the sign of the detuning; gravity effects in a vertical mazer for resonant and nonresonant interactions in the stationary regime were also studied in Refs. [9,10].

Another approach to the study of the motion of a cold atom coupled to the cavity field is the use of the adiabatic approximation with the dressed-atom point of view [15]. This was first introduced in Ref. [16], where it was shown that, for a large detuning, a sufficiently slow atom follows adiabatically the dressed levels which act as potentials that decelerate or accelerate the atom (here there is no quantum treatment of the center-of-mass motion). Later, using a similar scheme, but with the center-of-mass motion now quantized, it was shown that the cavity field acts as a refractive index medium for the atom and vice versa [17]. An analytical criterion to measure the validity of the aforementioned adiabatic approximation was analyzed in Ref. [18]. There it was shown that the adiabatic approximation is suitable for certain ranges of the parameters for the Gaussian and sinusoidal cavity modes.

In this article we consider a two-level atom with its center-of-mass motion quantized in one dimension (1D) coupled to a single-mode cavity field without dissipation. The system at hand is tripartite and is constituted by the spatial or center-of-mass degrees of freedom, the internal atom degrees of freedom, and the cavity-field degrees of freedom. Of these, two are discrete (the two levels of the atom and the number of photons in the given mode of the cavity field) and the third is a continuous one (the 1D spatial degree of freedom). The objective of this work is to analyze in detail the time evolution of various properties of the system (both as a whole or when information about some degrees of freedom is traced out) as the atom with a nonzero initial mean momentum enters the cavity-field region, transits it, and exits. In particular, we seek to characterize the type of entanglement and the degree of mixing exhibited by the various components of the system. Previous studies have been devoted to bipartite entanglement in the semiclassical [19] and dispersive [20] regimes or with emphasis in the transmission-resonance [21] regimes. Here, we study the time evolution of the entanglement between the different parts of the fully quantized system in several regimes. Moreover, we are interested in describing how the probability of emission evolves as the atom transits the cavity-field region. We also study the wave-packet structure and dynamics in search of matter wave precursors, echolike effects, and transmission resonances. The dependence of all these properties on the initial mean momentum of the atom, and the cavity frequency detuning with respect to the atomic transition, is also studied. Our highly precise numerical analysis does not rely on the adiabatic approximation.

The article is organized as follows. In Sec. II, the Hamiltonian modeling the system is presented, and the basic equations used to describe the temporal evolution of the system and of its properties are established. In Sec. III, the semiclassical

adiabatic approximation (SCAA) is briefly presented in order to compare and analyze qualitatively results when the center-of-mass motion is treated quantum mechanically. In Sec. IV, the numerical method and the parameters used to solve the equations established in Sec. II are briefly described. In Sec. V, the results are presented and discussed. In particular, the intermediate, cold, and transmission-resonance regimes (names originally coined in Ref. [4]) are considered, and the cases for which the cavity-field frequency is resonant and nonresonant with the atomic transition frequency, for blue and red detuning, are treated. Finally, the main results are summarized in Sec. VI.

II. THE MODEL

We consider a two-level atom with transition frequency ω_A coupled to a single mode of a cavity with frequency ω_L. The atom-field Hamiltonian in the long-wavelength and the rotating-wave approximations and in the dipole representation takes the form

$$H = \frac{1}{2M}\mathbf{P}^2 + \frac{\hbar\omega_A}{2}\sigma_3 + \hbar\omega_L\left(a^\dagger a + \frac{1}{2}\right)$$
$$+ \hbar g_0 u(\mathbf{R})(a^\dagger\sigma + \sigma^\dagger a). \qquad (1)$$

Here g_0 is the coupling strength for the interaction between the quantized field and the atom, u is the mode function of the cavity field, $\sigma = |g\rangle\langle e|$ is the atomic lowering operator, $\sigma_3 = |e\rangle\langle e| - |g\rangle\langle g|$ is the atomic inversion operator ($|e\rangle$ denotes the atom excited state, $|g\rangle$ the ground state), $a(a^\dagger)$ is the cavity-field annihilation (creation) operator, M is the atomic mass, and $\mathbf{R}$ and $\mathbf{P}$ are the center-of-mass position and momentum operators, respectively.

A constant of the motion for this Hamiltonian is $N_c = a^\dagger a + (1/2)\sigma_3 + (1/2)$. Using N_c we can transform to an interaction picture (IP) where the Hamiltonian takes the form

$$H_I = \frac{1}{2M}\mathbf{P}^2 - \frac{\hbar\delta_L}{2}\sigma_3 + \hbar g_0 u(\mathbf{R})(a^\dagger\sigma + \sigma^\dagger a), \quad (2)$$

where $\delta_L = \omega_L - \omega_A$ is the detuning between the cavity-field frequency and the atomic transition frequency. The IP Schrödinger equation is

$$i\hbar\frac{d}{dt}|\psi(t)\rangle = H_I|\psi(t)\rangle. \qquad (3)$$

The eigenvalues of the constant of the motion N_c are $0,1,2,...$ and the corresponding eigensubspaces are spanned, respectively, by the sets

$$\beta_{-1} = \{|\mathbf{r}\rangle|g\rangle|0\rangle : \mathbf{r}\in\mathbb{R}^3\},$$

and

$$\beta_n = \{|\mathbf{r}\rangle|\pm,n\rangle : \mathbf{r}\in\mathbb{R}^3\} \qquad (n = 0,1,2,\ldots). \quad (4)$$

Here $|\mathbf{r}\rangle$ is the eigenvector of $\mathbf{R}$, $|n\rangle$ ($n = 0,1,2,\ldots$) is a cavity-field Fock state, and we have introduced the kets

$$|\pm,n\rangle = \frac{1}{\sqrt{2}}(|e\rangle|n\rangle \pm |g\rangle|n+1\rangle) \qquad (n = 0,1,\ldots), \quad (5)$$

which together with $|g\rangle|0\rangle$ span the state space of the cavity field and the two levels of the atom. In the rest of the article we

will restrict to the subspace spanned by a particular β_n ($n = 0,1,2,...$).

The vectors in (4) allow us to express an arbitrary ket $|\psi\rangle$ in the subspace spanned by β_n in the following form:

$$|\psi\rangle = |\psi_{+n}\rangle|+,n\rangle + |\psi_{-n}\rangle|-,n\rangle, \qquad (6)$$

where $|\psi_{\pm n}\rangle$ are kets in the center-of-mass state space. Using decomposition (6) it is easy to see that (3) is equivalent to the following set of coupled equations

$$i\hbar\frac{d}{dt}|\psi_{\pm n}(t)\rangle = \left[\frac{1}{2M}\mathbf{P}^2 \pm V_n(\mathbf{R})\right]|\psi_{\pm n}(t)\rangle$$
$$- \frac{\hbar\delta_L}{2}|\psi_{\mp n}(t)\rangle, \qquad (7)$$

where $V_n(\mathbf{R}) = \hbar\sqrt{n+1}g_0 u(\mathbf{R})$. Equation (7) is the basis of all the calculations that follow.

A very important special case occurs when the atom is in resonance with the cavity field ($\delta_L = 0$). As discussed in Refs. [1–4], the set of Eq. (7) becomes equivalent to that of two independent particles without internal structure, one moving in the potential $V_n(\mathbf{R})$ with (non-normalized) state $|\psi_{+n}(t)\rangle$ and the other moving in the potential $-V_n(\mathbf{R})$ with (non-normalized) state $|\psi_{-n}(t)\rangle$, since it is easy to show that in this case $\langle\psi_{+n}(t)|\psi_{+n}(t)\rangle$ and $\langle\psi_{-n}(t)|\psi_{-n}(t)\rangle$ are constant in time. In the following we will make continuous use of this equivalence in the resonant case.

In general, we can identify three situations depending on how the initial mean kinetic energy K_0 of the atom is compared with the height $\hbar\sqrt{n+1}g_0$ of the potential (we assume that the maximum value of $u(\mathbf{r})$ is 1, as will be the case of our mode function). Following Refs. [4] and [8], we will refer to these different situations as the *cold atom or mazer regime* when $K_0 \ll \hbar\sqrt{n+1}g_0$, the *intermediate regime* when $K_0 \sim \hbar\sqrt{n+1}g_0$, and the *hot atom or Rabi regime* when $K_0 \gg \hbar\sqrt{n+1}g_0$.

We will now give expressions for several properties of the system that will enlighten the interpretation of the results in Sec. V. These expressions are general in the sense that they are valid whenever one restricts to the subspace spanned by β_n for some $n = 0,1,...$ and in one, two, or three dimensions.

Given that the initial state of the system is pure and belongs to the subspace spanned by β_n, using (6) the density operator $\rho(t)$ of the system can be expressed in the form

$$\rho(t) = [|\psi_{+n}(t)\rangle|+,n\rangle + |\psi_{-n}(t)\rangle|-,n\rangle]$$
$$\times [\langle\psi_{+n}(t)|\langle+,n| + \langle\psi_{-n}(t)|\langle-,n|]. \qquad (8)$$

The corresponding center-of-mass reduced density operator $\rho_{c.m.}(t)$ is obtained by tracing $\rho(t)$ over the internal atom and field degrees of freedom; the internal $\rho_{int}(t)$ and field $\rho_F(t)$ reduced density operators are obtained similarly.

Using (8) it is easy to show that the probability to find the atom in the excited state $|e\rangle$ at time t is given by the following expression:

$$P_e(t) = \tfrac{1}{2} + \text{Re}\langle\psi_{+n}(t)|\psi_{-n}(t)\rangle, \qquad (9)$$

where Re denotes the real part. Also, it is easily shown that the expected value $\langle\sigma_3\rangle(t)$ of the atomic inversion and the expected value $\langle a^\dagger a\rangle(t)$ of the photon number depend on

$P_e(t)$ in the following way

$$\langle\sigma_3\rangle(t) = 2P_e(t) - 1, \quad \langle a^\dagger a\rangle(t) = n + 1 - P_e(t). \quad (10)$$

Note that when $n = 0$ the expected number of photons $\langle a^\dagger a\rangle(t)$ is equal to the probability of emission $P_{em}(t)$.

Ever since it was realized that the entanglement present in quantum systems could be harnessed as a resource to transmit and store information, there has been great interest to characterize and manipulate it in many systems such as the micromaser [22]. One of our goals is to determine the type of entanglement present in the system under consideration and to quantify the degree of mixing in the various parts of it. For the latter, we take as figure of merit the linear entropies:

$$\begin{aligned} S_L^{c.m.}(t) &= 1 - \mathrm{Tr}_{c.m.}\rho_{c.m.}^2(t), \\ &= 1 - \langle\psi_{+n}(t)|\psi_{+n}(t)\rangle^2 - \langle\psi_{-n}(t)|\psi_{-n}(t)\rangle^2 \\ &\quad - 2|\langle\psi_{+n}(t)|\psi_{-n}(t)\rangle|^2, \end{aligned} \quad (11)$$

measures the degree of mixing between the internal atom and field degrees of freedom, and

$$S_L^F(t) = 1 - \mathrm{Tr}_F\rho_F^2(t) = 2P_e(t)[1 - P_e(t)], \quad (12)$$

measures the degree of mixing between the center-of-mass internal atom degrees of freedom. The linear entropy $S_L^{int}(t)$ of $\rho_{int}(t)$ yields an expression exactly equal to (12) and measures the degree of mixing between the center-of-mass and field degrees of freedom. Notice that a nonzero value of one of these linear entropies can be used as an indicator for the presence of entanglement between the nontraced degree of freedom and a traced degree of freedom.

To quantify the amount of entanglement between the internal atom and field degrees of freedom we will use the entanglement of formation $E_F(t)$. Since the dynamics are restricted to the subspace spanned by β_n, the cavity field can only have n or $n + 1$ photons. Therefore the cavity field is formally equivalent to a two-level system, and we can use the concurrence $C(t)$ to determine the entanglement of formation between atom and field [23]:

$$E_F(t) = s\left(\frac{1 + \sqrt{1 - C^2(t)}}{2}\right),$$

$$s(x) = -x\log_2 x - (1 - x)\log_2(1 - x), \quad (13)$$

where $C(t) = \max\{0, \sqrt{\lambda_1} - \sqrt{\lambda_2} - \sqrt{\lambda_3} - \sqrt{\lambda_4}\}$ and $\lambda_1 \geqslant \lambda_2 \geqslant \lambda_3 \geqslant \lambda_4$ are the eigenvalues of the matrix

$$\mathcal{C}(t) = [\rho_{int+F}(t)](\sigma_y \otimes \sigma_y)[\rho_{int+F}(t)]^*(\sigma_y \otimes \sigma_y). \quad (14)$$

Here σ_y is the well-known Pauli matrix and $[\rho_{int+F}(t)]^*$ is the element-wise complex conjugate of the density matrix $[\rho_{int+F}(t)]$ of the internal atom and field degrees of freedom. The matrix $[\rho_{int+F}(t)]$ is obtained by tracing $\rho(t)$ over the center-of-mass degrees of freedom and choosing a matrix representation.

It is easy to show that the concurrence $C(t)$ takes the form

$$C(t) = \sqrt{\frac{1}{2}A + \lambda\sqrt{P_e(t)[1 - P_e(t)]}}$$
$$\quad - \sqrt{\frac{1}{2}A - \lambda\sqrt{P_e(t)[1 - P_e(t)]}}, \quad (15)$$

where

$$\lambda = \sqrt{[\langle\psi_{+n}(t)|\psi_{+n}(t)\rangle - \langle\psi_{-n}(t)|\psi_{-n}(t)\rangle]^2 + 4[\mathrm{Im}\langle\psi_{+n}(t)|\psi_{-n}(t)\rangle]^2} \quad (16)$$

and

$$\begin{aligned} A &= \langle\psi_{+n}(t)|\psi_{+n}(t)\rangle^2 + \langle\psi_{-n}(t)|\psi_{-n}(t)\rangle^2 \\ &\quad - 2\mathrm{Re}[\langle\psi_{+n}(t)|\psi_{-n}(t)\rangle^2]. \end{aligned} \quad (17)$$

Im denotes the imaginary part.

III. SEMICLASSICAL ADIABATIC APPROXIMATION

The SCAA, briefly presented in this section, gives a simple physical picture that allows one to understand qualitatively how the atom should move and how the system should behave in general terms when several conditions (to be explained below) are satisfied. In this approximation the equations to be solved in any particular problem are ordinary instead of partial. The SCAA is presented in order to determine how well its predictions compare with the exact results based on a full quantum treatment and to understand qualitatively why the system behaves in a particular way for certain values of the parameters.

When both the spatial extension of the center-of-mass wave packet and the de Broglie wavelength of the atom are much smaller than the rest of the lengths of the system, a semiclassical approximation can be used to treat the

center-of-mass motion of the atom [16]. The center-of-mass trajectory $\mathbf{r}(t)$ defines the time-dependent Hamiltonian

$$\begin{aligned} H_{AD}(t) &= \frac{\hbar\omega_A}{2}\sigma_3 + \hbar\omega_L\left(a^\dagger a + \frac{1}{2}\right) \\ &\quad + \hbar g_0 u[\mathbf{r}(t)](a^\dagger\sigma + \sigma^\dagger a), \end{aligned} \quad (18)$$

which determines the evolution of the internal atom and field degrees of freedom. This Hamiltonian has instantaneous eigenvalues

$$E_{\pm n}[\mathbf{r}(t)] = \hbar(n + 1)\omega_L \pm \frac{\hbar}{2}\Omega_n[\delta_L, \mathbf{r}(t)] \quad (19)$$

and corresponding instantaneous eigenvectors

$$|1, n, t\rangle = \cos\left[\frac{\theta_n(t)}{2}\right]|e, n\rangle + \sin\left[\frac{\theta_n(t)}{2}\right]|g, n + 1\rangle,$$

$$|2, n, t\rangle = -\sin\left[\frac{\theta_n(t)}{2}\right]|e, n\rangle + \cos\left[\frac{\theta_n(t)}{2}\right]|g, n + 1\rangle, \quad (20)$$

where

$$\Omega_n[\delta_L, \mathbf{r}(t)] = \sqrt{\delta_L^2 + 4(N + 1)g_0^2 u[\mathbf{r}(t)]^2},$$

$$\tan\theta_n(t) = -2\sqrt{n + 1}g_0 u[\mathbf{r}(t)]/\delta_L(0 \leqslant \theta_n(t) \leqslant \pi). \quad (21)$$

In particular, it is easy to see that for zero detuning

$$|j,n,t\rangle = \begin{cases} |+,n\rangle & \text{if } j = 1, \\ -|-,n\rangle & \text{if } j = 2. \end{cases} \tag{22}$$

The adiabatic approximation is now invoked: If the reduced system that just describes the internal atom plus field degrees of freedom is initially prepared in an eigenvector $|j,n,t_0\rangle$ of $H_{\text{AD}}(t_0)$, then it will approximately evolve to $|j,n,t\rangle$, and the properties of this reduced system can be determined using $|j,n,t\rangle$. Also, $E_{\pm n}[\mathbf{r}(t)]$ (plus for $j = 1$, minus for $j = 2$) act as potentials under which the center-of-mass moves and the semiclassical evolution equation for $\mathbf{r}(t)$ consistent with the Hamiltonian $H_{\text{AD}}(t)$ is

$$M\frac{d^2\mathbf{r}}{dt^2} = -\boldsymbol{\nabla} E_{\pm n}[\mathbf{r}(t)]. \tag{23}$$

Lets suppose that $u(\mathbf{r}) \to 0$ as $|\mathbf{r}| \to +\infty$ (such as the case we will be considering). Then it is easy to show that

$$|1,n,t\rangle \to \begin{cases} |e,n\rangle & \text{if } \delta_L < 0, \\ -|g,n+1\rangle & \text{if } \delta_L > 0, \end{cases}$$
$$|2,n,t\rangle \to \begin{cases} -|e,n\rangle & \text{if } \delta_L > 0, \\ -|g,n+1\rangle & \text{if } \delta_L < 0, \end{cases} \tag{24}$$

as $|\mathbf{r}| \to +\infty$. Suppose now that the reduced system that just describes the internal atom plus the field degrees of freedom is initially prepared in the state $|e,n\rangle$ in a region where $u(\mathbf{r})$ is negligible. Then the reduced system will be found in the eigenstate $|j,n,t_0 = 0\rangle$ of H_{AD} according to (24) if $\delta_L \neq 0$, and it will follow adiabatically the state $|j,n,t\rangle$ as the atom moves under the corresponding potential $E_{\pm n}(\mathbf{r})$. Note that this picture cannot be used when $\delta_L = 0$ since, according to (5) and (24), $|e,n\rangle$ is not even approximately an eigenstate of (18) when $u(\mathbf{r})$ is negligible.

We end this section with a caveat. The SCAA must not be be confused with the quantum adiabatic approximation (QAA) [17,18]. The former describes the center-of-mass motion classically by means of Eq. (23) and the internal atom and field state by (20). Meanwhile, the QAA describes the state of the system as

$$\phi_1(\mathbf{r},t)|1,n,\mathbf{r}\rangle + \phi_2(\mathbf{r},t)|1,n,\mathbf{r}\rangle \tag{25}$$

with

$$|1,n,\mathbf{r}\rangle = \cos\left[\frac{\theta_n(\mathbf{r})}{2}\right]|e,n\rangle + \sin\left[\frac{\theta_n(\mathbf{r})}{2}\right]|g,n+1\rangle,$$
$$|2,n,\mathbf{r}\rangle = -\sin\left[\frac{\theta_n(\mathbf{r})}{2}\right]|e,n\rangle + \cos\left[\frac{\theta_n(\mathbf{r})}{2}\right]|g,n+1\rangle,$$
$$\tan\theta_n(\mathbf{r}) = -2\sqrt{n+1}\,g_0 u(\mathbf{r})/\delta_L \quad (0 \leqslant \theta_n(\mathbf{r}) \leqslant \pi), \tag{26}$$

and consists in evolving the wave packets $\phi_1(\mathbf{r},t)$ and $\phi_2(\mathbf{r},t)$ [differing from the $\langle\mathbf{r}|\psi_{\pm n}(t)\rangle$ used in this article, Eq. (7)] under independent Schrödinger equations of the form

$$i\hbar\frac{d}{dt}\phi_j(\mathbf{r},t) = \left[-\frac{\hbar^2}{2M}\nabla^2 + V_j(\mathbf{r})\right]\phi_j(\mathbf{r},t), \quad j = 1,2, \tag{27}$$

with potentials $V_j(\mathbf{r})$ of the form in Eq. (19) with $\mathbf{r}(t)$ replaced by $\mathbf{r}$. This approximation has the advantage of taking as a

starting point quantum decoupled equations when there is nonzero detuning. Its range of validity was studied in detail in Ref. [18]. Here we shall not use this approximation since our exact treatment of partial differential equations does not require it.

IV. THE NUMERICAL SIMULATION

For the numerical simulation we will restrict to one dimension, which will be taken to be the z direction. Furthermore, we will restrict to the subspace spanned by β_0 (that is the cavity field will be able to have only zero or one photons). A complete quantum treatment in the coordinate representation of Eqs. (7) requires solving the equations

$$i\hbar\frac{\partial}{\partial t}\psi_{\pm 0}(z,t) = \left[-\frac{\hbar^2}{2M}\frac{\partial^2}{\partial z^2} \pm V_0(z)\right]\psi_{\pm 0}(z,t)$$
$$-\frac{\hbar\delta_L}{2}\psi_{\mp 0}(z,t), \tag{28}$$

where $V_0(z) = \hbar g_0 u(z)$.

We solved numerically equations (28) by the method of lines (MOL) [24–26] with an adaptive spatial grid. The advantage of the MOL solution is that we can *see* the wave packets evolve, that is, we can see how they advance, transit the cavity, exit, and deform in the process. Also, the wave functions in the momentum representation were reconstructed using the fast Fourier transform and the Shannon sampling theorem [27].

As for the parameters of our numerical simulation, we took $\lambda_A = 2\pi c/\omega_A = 780 \times 10^{-9}$ m for the wavelength of the atomic transition, $g_0 = 2\pi \times 16 \times 10^6$ s^{-1}, and $M = 1.4 \times 10^{-25}$ kg. We considered a Gaussian cavity mode function

$$u(z) = e^{-z^2/w_0^2}, \tag{29}$$

whose standard deviation is $w_0/\sqrt{2}$. This continuous potential is considered a good approximation for an open cavity mode. It was first studied numerically in the context of CQED for stationary states and zero detuning [28]. Later, transmission effects due to wave-packet dynamics were explored both for zero and red detuned atom-field interactions [21]. The waist of the mode w_0 will be taken as 10^{-6} m in general, with the exception of the analysis of the transmission resonances (treated in Sec. V D) where it will be varied. These values of the parameters correspond to the experiments with Rubidium 85 described in Ref. [29], excluding w_0, which in that experimental setup has the value $w_0 = 29 \times 10^{-6}$ m. Our w_0 values correspond to highly focused modes. We will show in the next section that many of our results are, nevertheless, independent of the value of w_0 when outside the transmission-resonance regime.

Initially, the atom was taken to be in the excited state, the cavity to contain zero photons and the center of mass to be described by a minimum-uncertainty Gaussian wave packet. That is, we took the initial state of the system to be the following separable state:

$$|\psi(0)\rangle = |\psi_{\text{c.m.}}\rangle|e\rangle|0\rangle, \tag{30}$$

where

$$\psi_{\text{c.m.}}(z) = \langle z | \psi_E \rangle = \left(\frac{1}{2\pi \Delta^2} \right)^4$$

$$\times \exp \left[-\frac{1}{4} \left(\frac{z - \mu}{\Delta} \right)^2 + ikz \right]. \quad (31)$$

Here μ is the expected value of the center-of-mass position, Δ is the standard deviation of the center-of-mass position, and $\hbar k$ is the mean momentum of the atom, all at time $t = 0$. For definiteness, we took these to be $\mu = -4w_0/\sqrt{2}$, $\Delta = \lambda_{\text{dB}}/4$ with λ_{dB} the initial mean de Broglie wavelength of the atom, $\lambda_{\text{dB}} = 2\pi/k = 2\pi\hbar/(Mv)$ with $v = \alpha\sqrt{2\hbar g_0/M}$ the initial mean velocity of the atom.

Using Eq. (5), Eq. (30) can be reexpressed in the form given by Eq. (6) as follows:

$$|\psi(0)\rangle = \frac{1}{\sqrt{2}} |\psi_{\text{c.m.}}\rangle |+, n = 0\rangle + \frac{1}{\sqrt{2}} |\psi_{\text{c.m.}}\rangle |-, n = 0\rangle. \quad (32)$$

With the exception of the analysis of the transmission resonances, we report numerical simulations for three different values of $\alpha = 1/10, 1/\sqrt{2}$, and $\sqrt{5/4}$. The initial kinetic energy for the first α is much smaller than the atom-field coupling energy $\hbar g_0$ (cold atom regime), while for the second and third cases it is in the order of the atom-field coupling energy (intermediate regime). These values of α give initial velocities of 3.9, 27, and 43 cm/s, respectively. Note that at time $t = 0$ we have $\Delta/\mu = 10^{-3}/\sqrt{\alpha}$ and $\Delta_p/(\hbar k) = 1/\pi$, where $\Delta_p = \hbar/(2\Delta)$ is the standard deviation of momentum at $t = 0$. Hence, the chosen values correspond to an atom initially very well localized in position (but not so much in momentum) which is slowly advancing from a region where the atom-field interaction is negligible toward the region where the cavity field is strongest. Also, for each of the aforementioned values of α we made numerical simulations for three different values of the detuning: $\delta_L = 0$, $\pm g_0/16$, with the latter corresponding to one third of the spontaneous emission rate for the experiments described in Ref. [29].

V. RESULTS

We now turn to discuss the results of the numerical simulations. In the following we will take the phrase *probability of being transmitted through the cavity field* to mean the probability to find the atom in the interval $(4w_0/\sqrt{2}, +\infty)$ once it has left the *interaction region*, that is, where the atom-field coupling has non-negligible values. We will take it to be the region centered at zero between -4 and $+4$ standard deviations of the Gaussian mode function in Eq. (29), $-4w_0/\sqrt{2} \leqslant z \leqslant 4w_0/\sqrt{2}$. Similarly, we will take the phrase *probability of being reflected by the cavity field* to mean the probability to find the atom in the interval $(-\infty, -4w_0/\sqrt{2})$ once it has left the interaction region. *Leaving the interaction region* is measured by the expected value of the position operator Z when there is nonzero detuning and by the quantities

$$\frac{\langle \psi_{\pm 0}(t) | Z | \psi_{\pm 0}(t) \rangle}{\langle \psi_{\pm 0}(t) | \psi_{\pm 0}(t) \rangle}, \quad (33)$$

when the system is in resonance. These can be interpreted as the expected value of the position of the particle that moves under the repulsive (attractive) potential when the plus (minus) sign is used. Evidently, these quantities depend on the structure of the wave packet.

For small values of the initial mean kinetic energy K_0 and certain values of the effective length of the interaction region L_{eff}, the asymptotic properties of the system, such as probability of emission and transmission through the cavity field, exhibit high sensibility in these parameters. These effects are associated in the literature to tunneling resonances [5,21,28]. Several of the assertions found to be valid outside the transmission-resonance regime do not hold there. In the next three subsections, we describe the evolution of the system outside that regime. We will group the results according to the sign of the detuning $\delta_L = \omega_L - \omega_A$. Transmission resonances will be treated in a fourth subsection.

A. Zero detuning outside the transmission-resonance regime

As expected, the atom's probability of being transmitted through the cavity field increases as the velocity rises. Our numerical simulations show that for the initial velocities $v = 3.9, 27$, and 43 cm/s the atom has respective transmission probabilities of 50, 51.4, and 84%. Note that in the case of the second initial velocity, the additional 1.4 to 50% in the transmission probability is due to tunneling of $|\psi_{+0}(t)\rangle$ through the repulsive potential $V_0(\mathbf{R})$, since the initial mean kinetic energy of the atom is half the height $\hbar g_0$ of the potential barrier [see Eqs. (31) and (32) and the paragraph that follows them]. Analogously, in the case of the third initial velocity, the missing 16 to 100% in the transmission probability is due to reflection of $|\psi_{+0}(t)\rangle$ by the repulsive potential $V_0(\mathbf{R})$, since the initial mean kinetic energy of the atom is $(1/4)\hbar g_0$ higher than the height $\hbar g_0$ of the potential barrier.

In the cold regime, the structure of the wave packets $\psi_{\pm 0}(z, t)$ is Gaussian-like for sufficiently long times for both the reflected and transmitted matter waves; Fig. 1(c). As for the corresponding position probability density function (PPDF), it has the structure of two quasi-Gaussian functions; Fig. 1(f). The numerical results show that, when the atom leaves the interaction region, the uncertainty in momentum recovers its initial value both for $\psi_{+0}(z, t)$ and for $\psi_{-0}(z, t)$, while their position uncertainty increases linearly in time although it is smaller than for a freely evolving wave packet.

In the intermediate regime, for the velocities $v = 27$ and 43 cm/s the uncertainties in momentum are asymptotically constant for both $\psi_{+0}(z, t)$ and $\psi_{-0}(z, t)$ but larger than their initial value. Also, the transmitted asymptotic packages are quasi-Gaussian [Figs. 1(i) and 1(o)]. The part of the center-of-mass wave function that moves in an attractive potential $\psi_{-0}(z, t)$ is transmitted with a simple Gaussian-like structure, while $\psi_{+0}(z, t)$ evolves with a very rich structure. As illustrated in Figs. 1(i) and 1(o) for velocities $v = 27$ and 43 cm/s, $\psi_{+0}(z, t)$ is divided into transmitted and reflected wave packets. The maximum of the transmitted part of $\psi_{+0}(z, t)$ for $v = 27$ cm/s [Fig. 1(i)] is evidently located at a farther position than the maximum of $\psi_{-0}(z, t)$, although it has a lower amplitude. That is the essence of the so-called precursors which have been widely discussed in the optics context [30]. The PPDF
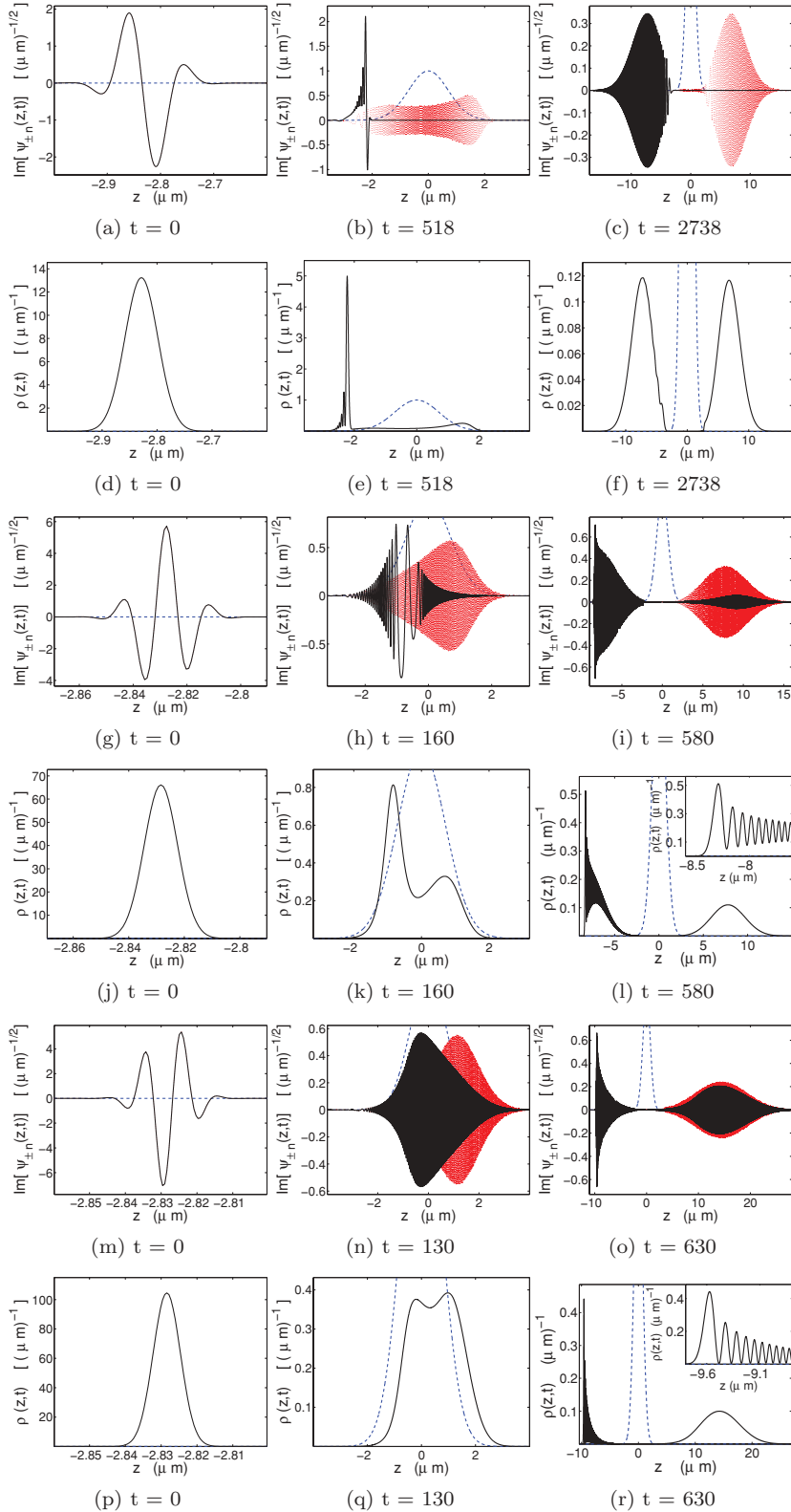
FIG. 1. (Color online) Evolution of the imaginary parts $Im[\psi_{+0}(z,t)]$ (black solid line) and $Im[\psi_{-0}(z,t)]$ (red dotted line) of the wave packets $\psi_{\pm 0}(z,t)$ and the position probability density functions (PPDF) $\rho(z,t)$ for zero detuning. The first two rows refer to the initial velocity $v = 3.9$ cm/s, the third and fourth rows to $v = 27$ cm/s, and the fifth and sixth rows to $v = 43$ cm/s. [(l) and (r)]A close-up of the reflected part of the PPDF is included. Time appears in units of $2\pi/g_0$ and the mode function $u(z)$ (blue dashedline) is drawn in all figures.

for the intermediate regime consists of an essentially Gaussian transmitted part and a reflected part that resembles a train of quasi-Gaussian packets, i.e., it has an echolike structure [Figs. 1(l) and 1(r)]. Observing the detailed time evolution of the PPDF [31], it is found that a Gaussian-like structure for the PPDF is preserved until the expected value of the position of the atom is approximately at the center of the

interaction region, after which it splits into a part that continues to traverse the cavity and another part that is reflected, as illustrated in Figs. 1(k) and 1(q). The echo structure comes about as a result of the interference between a portion of the wave packet $\psi_{+0}(z,t)$ that is still advancing toward the center of the interaction region and another part of it that moves in the opposite direction. Furthermore, the echo
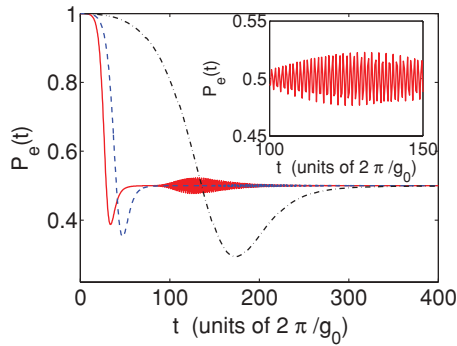
FIG. 2. (Color online) The probability of finding the atom in the excited state at time t for the initial velocities $v = 3.9$ (black dash-dot line), 27 (blue dashed line), and 43 (red solid line) cm/s for zero detuning. Rabi-like oscillations are observable just for the highest velocity as can be observed in the close-up shown in the inside figure. Time appears in units of $2\pi/g_0$.

structure is preserved well outside the interaction region in the intermediate regime.

We will now discuss the rest of the evaluated properties. As can be seen from Fig. 2, the probability to find the atom in the excited state $P_e(t)$ contrasts sharply with that obtained when the center-of-mass motion is not quantized. In resonance, the latter exhibits the well-known Rabi oscillations which have been ingeniously used in the preparation of predetermined quantum states of the internal atomic degrees of freedom and the cavity field (see, e.g., Ref. [22]). Meanwhile, when the center-of-mass motion requires a quantized description, the Rabi oscillations tend to disappear. For the smallest initial velocity, they disappear completely and the probability of emission is always less than 1 (Fig. 2). This can be explained easily by looking at Eq. (9) and Fig. 1(b). Since $|\psi_{+0}(t)\rangle$ evolves under the repulsive potential and $|\psi_{-0}(t)\rangle$ evolves under the attractive potential, the first is quickly reflected [see the times in Figs. 1(a)–1(c)] while the second is transmitted through the cavity field. Therefore, the overlap between $|\psi_{+0}(t)\rangle$ and $|\psi_{-0}(t)\rangle$ rapidly goes to zero and there is no chance for oscillations as the probability of finding the atom in the excited state rapidly reaches a stationary value of $1/2$. This phenomenon is also observed for the higher initial velocities,

but small oscillations start to appear as $|\psi_{+0}(t)\rangle$ penetrates the barrier further and is mostly transmitted as occurs for the highest reported velocity [Fig. 1]. This also makes the overlap $\langle\psi_{+0}(t)|\psi_{-0}(t)\rangle$ persist longer, but the delay between $|\psi_{+0}(t)\rangle$ and $|\psi_{-0}(t)\rangle$ ultimately decreases it to negligible values. The delay can be measured by the difference between the expectation values of the position for $|\psi_{+0}(t)\rangle$ and $|\psi_{-0}(t)\rangle$, Eq. (33). The small oscillations exhibited mostly in the case with the highest initial velocity appear to be the onset of the aforementioned Rabi oscillations.

The expected values of the atomic inversion and photon number, Eq. (10), as well as the linear entropy between the internal and center-of-mass degrees of freedom, Eq. (12), can be obtained directly from $P_e(t)$. On the other hand, entanglement between the internal atom degrees of freedom and the cavity field is also highly affected by the quantization of the center-of-mass motion. As illustrated in Fig. 3(a), as soon as the atom enters the interaction region the entanglement of formation between the internal atom degrees of freedom and the cavity field grows to a large value and then rapidly becomes negligible [see the times in Figs. 1 and 3(a)]. On the other hand, if the center-of-mass motion is treated classically and there is zero detuning [22], the latter presents many oscillations between zero and 1 corresponding to the cases where the atom is in the ground or excited state and when the atom-field system is in the states $|\pm,0\rangle$, respectively. This can easily be understood if we refer to Eqs. (15) and (16). For the configuration under consideration we have for any time t

$$\langle\psi_{+0}(t)|\psi_{+0}(t)\rangle = \langle\psi_{-0}(t)|\psi_{-0}(t)\rangle = \tfrac{1}{2}. \qquad (34)$$

Then, using Eqs. (15) and (16), it can be shown that the concurrence $C(t)$ approaches the value zero as soon as the overlap between $|\psi_{+0}(t)\rangle$ and $|\psi_{-0}(t)\rangle$ becomes negligible. Hence, the entanglement of formation takes the value of zero and there is no entanglement between the internal atom degrees of freedom and the cavity field.

As illustrated in Fig. 3, the reduced density operators $\rho_{c.m.}(t)$ and $\rho_F(t)$ rapidly acquire a maximum-mixed state structure (see the times in Figs. 1 and 3). This can be explained by taking a glance at Eqs. (11) and (12). Using Eq. (34) it is seen that $S_L^{c.m.}(t)$ and $S_L^F(t)$ take on their maximum values as
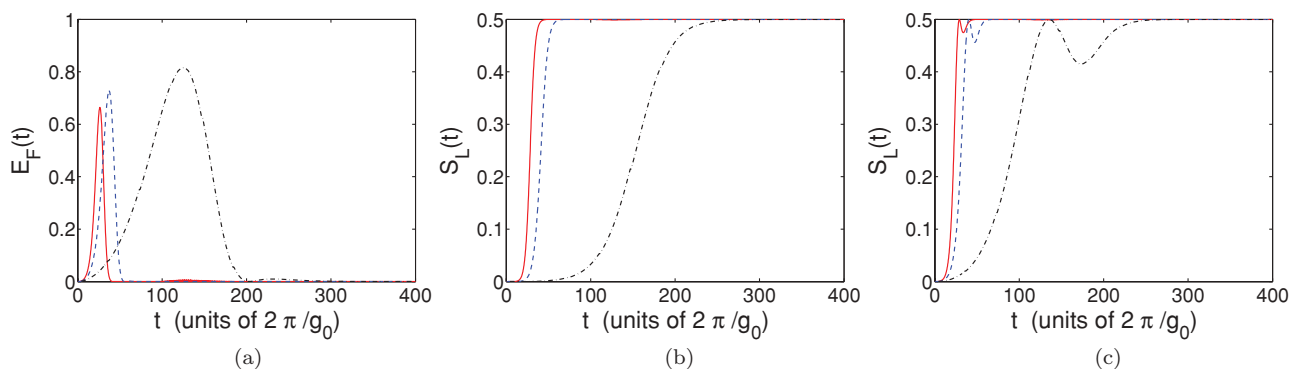
FIG. 3. (Color online) (a) Entanglement of formation between the internal atom degrees of freedom and the cavity field; (b) linear entropy for the internal atom degrees of freedom and the cavity field; (c) linear entropy for the center of mass and internal atom degrees of freedom. Results are shown for zero detuning and initial velocities $v = 3.9$ (black dash-dot line), 27 (blue dashed line), and 43 (red solid line) cm/s. Time is in units of $2\pi/g_0$.
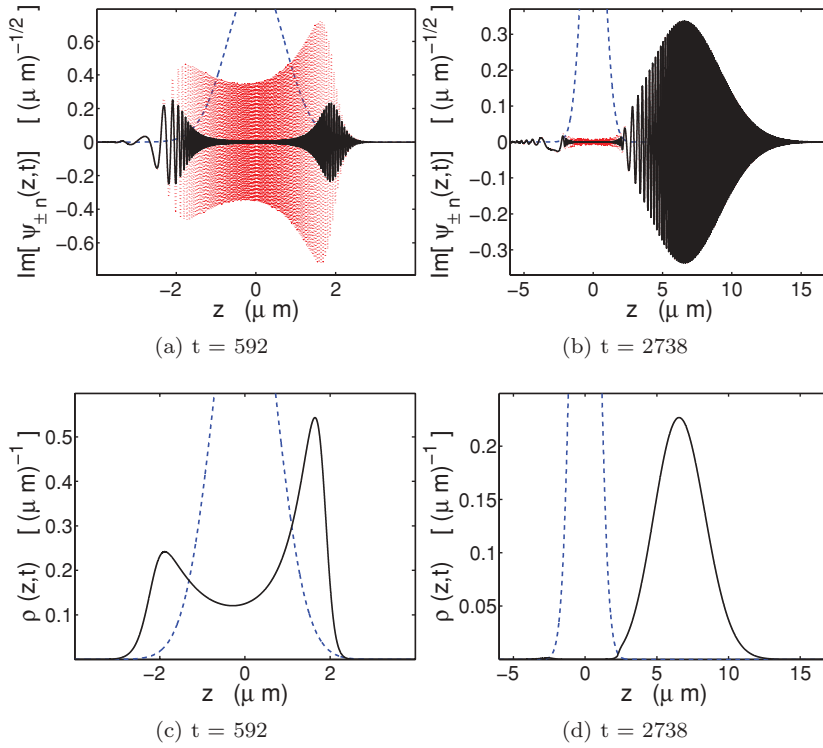
FIG. 4. (Color online) The first row illustrates the evolution of the imaginary parts $\text{Im}[\psi_{+0}(z,t)]$ (black solid line) and $\text{Im}[\psi_{-0}(z,t)]$ (red dotted line) of the wave packets $\psi_{\pm0}(z,t)$ for blue detuning, $\delta_L = g_0/16$. The initial velocity is $v = 3.9$ cm/s and the initial state is the same as in Fig. 1(a). The real parts behave similarly. The second row illustrates the evolution of the PPDF for the same initial velocity and state used in Fig. 1(d). Time appears in units of $2\pi/g_0$ and the mode function $u(z)$ (blue-dashed line) is drawn in all figures.

soon as the overlap between $|\psi_{+0}(t)\rangle$ and $|\psi_{-0}(t)\rangle$ becomes negligible.

As we will now show, the consequence of the aforementioned asymptotic zero entanglement of formation and nonzero linear entropies is that the system exhibits not only tripartite entanglement but also genuine tripartite entanglement [32]. This means that given a tripartite pure state, all of its bipartite reductions yield mixtures of separable pure states. The best known example of this is the Greenberger-Horne-Zeilinger (GHZ) system [32].

Consider an initial state of the form

$$|\psi_0\rangle = |\psi_{\text{c.m.}}\rangle(c_1|e,n\rangle + c_2|g,n+1\rangle), \qquad (35)$$

with $|c_1|^2 + |c_2|^2 = 1$, $c_1 c_2 = 0$, and $\langle\psi_{\text{c.m.}}|\psi_{\text{c.m.}}\rangle = 1$. Then it is easily seen that whenever $\langle\psi_{+n}(t)|\psi_{-n}(t)\rangle = 0$, the reduced density operators for the internal atom plus field (int + F), center of mass plus internal atom (c.m. + int) and center of mass plus field (c.m. + F) degrees of freedom are, respectively:

$$\rho_{\text{int}+F}(t) = \tfrac{1}{2}|e\rangle\langle e| \otimes |n\rangle\langle n| + \tfrac{1}{2}|g\rangle\langle g| \otimes |n+1\rangle\langle n+1| \qquad (36)$$

$$\rho_{\text{c.m.}+\text{int}}(t) = \tfrac{1}{2}P_+(t) \otimes |e\rangle\langle e| + \tfrac{1}{2}P_-(t) \otimes |g\rangle\langle g|, \qquad (37)$$

$$\rho_{\text{c.m.}+F}(t) = \tfrac{1}{2}P_+(t) \otimes |n\rangle\langle n| + \tfrac{1}{2}P_-(t) \otimes |n+1\rangle\langle n+1|, \qquad (38)$$

where $P_\pm(t)$ are density operators defined by

$$P_\pm(t) = [|\psi_{+n}(t)\rangle \pm |\psi_{-n}(t)\rangle][\langle\psi_{+n}(t)| \pm \langle\psi_{-n}(t)|]. \qquad (39)$$

Note that (36) is a separable maximum mixed state, since its linear entropy takes on its largest value of $1/2$. Furthermore,

(37) and (38) are also separable mixed states since $P_\pm(t)$ represent orthogonal pure states. Therefore, the system exhibits genuine tripartite entanglement. This is precisely the case we have at hand with $n = 0$.

It is important to note that many of the phenomena described, e.g., the disappearance of the Rabi oscillations and the existence of genuine tripartite entanglement, rely on two things: an initial state of the form (35) and $\langle\psi_{+n}(t)|\psi_{-n}(t)\rangle = 0$ for the time interval of interest. Therefore it is a phenomenon that would be observed for positive mode functions $u(\mathbf{r})$ and in one to three dimensions as long as the two aforementioned conditions are satisfied.

B. Blue detuning outside the transmission-resonance regime

The wave-packet dynamics in the case of blue detuning exhibit interesting features that may be unseen in approximate treatments (Fig. 4). For all initial mean momenta, $\psi_{+0}(z,t)$ decreases its amplitude and almost disappears inside the interaction region while $\psi_{-0}(z,t)$ increases accordingly, an effect due to the coupled equations that describe them. Later, as the wave packets exit the interaction region, $\psi_{+0}(z,t)$ reappears so that asymptotically $\psi_{+0}(z,t) = \psi_{-0}(z,t)$, an equality obtained numerically and expected from analytical considerations given below. In all numerical simulations we performed, the wave packets and the position probability density function eventually become quasi-Gaussian (Fig. 4), and the expected values of the momentum and its uncertainty are asymptotically found to approach their initial values.

For blue detuning, if one uses the SCAA presented in Sec. III, it is expected that the atom is transmitted through the cavity field for all initial momenta. The reason for this is
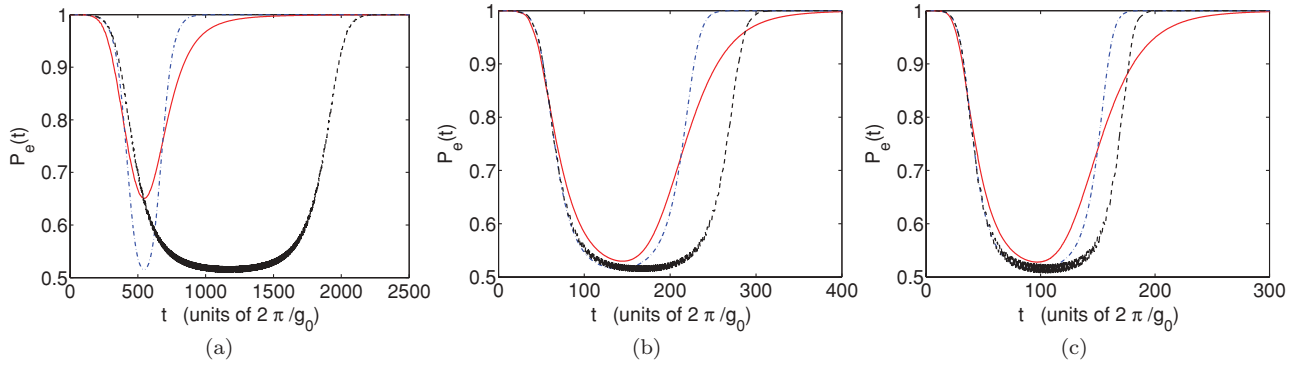
FIG. 5. (Color online) The probability of finding the atom in the excited state for blue detuning, $\delta_L = g_0/16$. Each part of the figure illustrates the result obtained when the center-of-mass motion is quantized (red solid line), treated in the semiclassical adiabatic approximation (blue dash-dot line), or, finally, follows the classical trajectory $z = vt + \mu$, where v is the initial velocity and μ the initial position (black dashed line). Results are shown for initial velocities (a) $v = 3.9$, (b) 27, and (c) 43 cm/s. Time is in units of $2\pi/g_0$.

that the atom moves under the attractive potential $E_{-0}(z)$ with an energy $E = (1/2)Mv^2 + E_{-0}(\mu)$ larger than the maximum height of $E_{-0}(z)$; see Eqs. (19)–(24) and the definition of μ and v in Sec. IV. This turns out to be the case also in the exact quantum treatment outside the transmission-resonance regime (analyzed in Sec. VD), since the probability of transmission results 100% for detunings such as $\delta_L = g_0/16$. Nevertheless, the SCAA is actually not strictly valid, because as the atom wave packets evolve their spatial extension becomes comparable to the size of the interaction region (Fig. 4), and the SCAA does not take into account this position dispersion. Consequently, the breakdown of that approximation reveals itself in the position probability density function (Fig. 4), and the quantitative predictions for the probability to find the atom in the excited state $P_e(t)$ (Fig. 5). Nevertheless, the SCAA does reproduce the inverted bell-like structure of $P_e(t)$ that becomes unity outside the interaction region and takes its minimum value when the expected value of the position of the atom is approximately at the center of the interaction region

(Figs. 5 and 6). These figures also illustrate the results when the approximation $z = vt + \mu$ is taken.

In the exact quantum treatment the asymptotic behavior of the linear entropies and the entanglement of formation (Fig. 7) is easily understood using the following argument. Consider a density operator of the form (8). If the probability of finding the atom in the excited state $P_e(t)$ is 1 and

$$\langle\psi_{+n}(t)|\psi_{+n}(t)\rangle = \langle\psi_{-n}(t)|\psi_{-n}(t)\rangle = \tfrac{1}{2}, \tag{40}$$

then, using the Cauchy-Schwarz inequality, necessarily $|\psi_{+n}(t)\rangle = |\psi_{-n}(t)\rangle$. From this it is easy to conclude that the whole system is in the following product state:

$$\rho(t) = 2|\psi_{+n}(t)\rangle\langle\psi_{+n}(t)| \otimes |e\rangle\langle e| \otimes |n\rangle\langle n|. \tag{41}$$

We note that this is precisely the case we have at hand, since $P_e(t) = 1$ and Eq. (40) is satisfied [Fig. 7(c)]. Inside the interaction region, the structure of the linear entropy between the internal atom and field degrees of freedom is understood
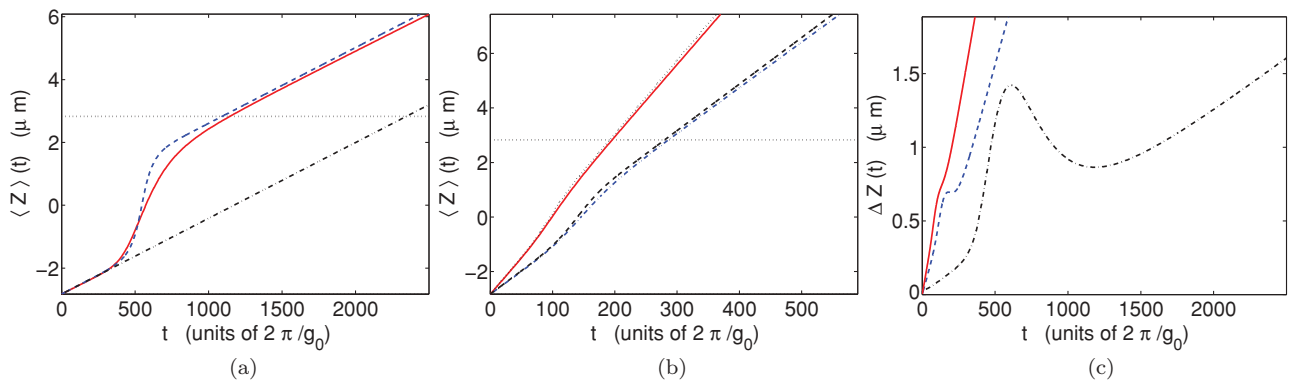
FIG. 6. (Color online) For blue detuning, $\delta_L = g_0/16$, (a) illustrates the expected value of the position of the atom when the center-of-mass motion is quantized with the initial velocity $v = 3.9$ cm/s (red solid line). Results for the adiabatic (blue dashed line) and $z = vt + \mu$ (black dash-dot line) treatments of the center-of-mass motion are also shown. (b) The expected values of the position of the atom with the initial velocity $v = 27$ cm/s for the fully quantum treatment (blue dash-dot line) and for the SCAA (black dashed line). Also shown is $\langle Z \rangle$ for the initial velocity 43 cm/s resulting from the full quantum treatment (red solid line) and for the SCAA (black dotted line). The horizontal dotted lines indicate the limits of the interaction region. (c) The standard deviation of the position of the atom when the center-of-mass motion is quantized with the initial velocities $v = 3.9$ cm/s (black dash-dot line), 27 cm/s (blue dashed line), and 43 cm/s (red solid line). In all figures time is in units of $2\pi/g_0$.
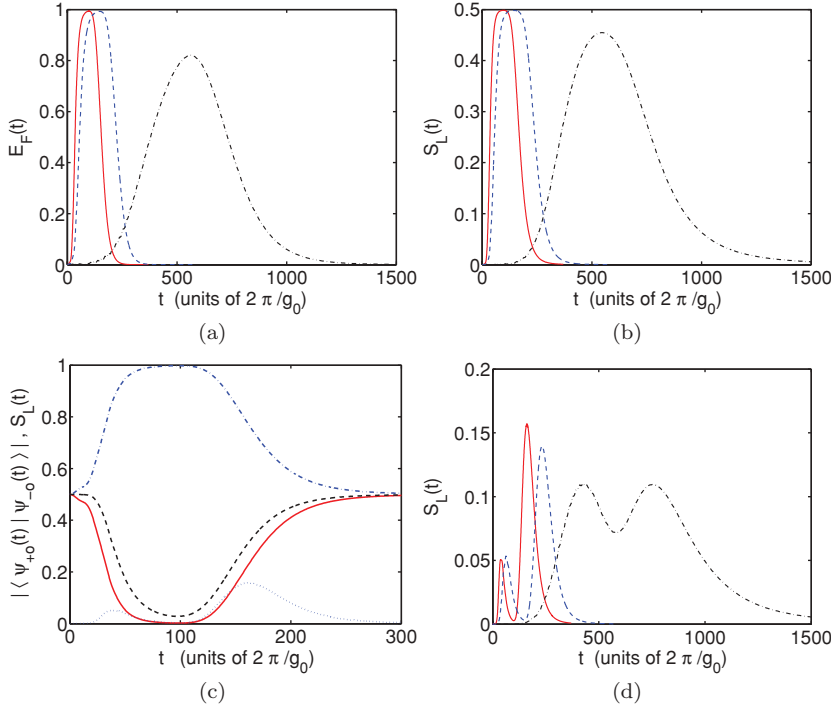
FIG. 7. (Color online) For blue detuning, $\delta_L = g_0/16$, (a) and (d) illustrate the evolution of the entanglement of formation and the linear entropy between the internal atom and field degrees of freedom, respectively. (b) The evolution of the linear entropy between the center-of-mass and internal atom degrees of freedom; it is exactly the same for the center-of-mass and field degrees of freedom. [(a), (b), and (d)] Results for initial velocities $v = 3.9$ cm/s (black dash-dot line), 27 cm/s (blue dashed line), and 43 cm/s (red solid line). (c) The evolution of the square of the norm of the wave functions $\psi_{+0}(z,t)$ (red solid line) and $\psi_{-0}(z,t)$ (blue dash-dot line), the modulus of the overlap $|\langle \psi_{+0}(z,t)|\psi_{-0}(z,t)\rangle|$ (black dashed line), and the linear entropy between the internal atom and field degrees of freedom (blue dotted line) for the largest initial velocity $v = 43$ cm/s. Time appears in units of $2\pi/g_0$.

by using Eq. (11) and Fig. 7(c). For the other velocities the graphics are similar.

If one uses the semiclassical adiabatic approximation, one expects that the system asymptotically has the atom in the excited state and the cavity field with zero photons. This is due to the fact that the system follows adiabatically the corresponding state, Eqs. (20) and (24). Therefore, one expects that the system is found asymptotically in a pure separable state. Although this does happen asymptotically in the exact quantum treatment outside the transmission-resonance regime (Fig. 7) the SCAA cannot describe quantitatively what happens inside the interaction region. The reason is that the SCAA is not strictly valid, as analyzed in the preceding paragraphs.

By writing the exact wave functions in terms of the states given by Eq. (26) one can obtain an estimate of the validity of the quantum adiabatic approximation (QAA). In this way, it is observed that for $\delta_L = g_0/16$ the exact wave function has always a dominant contribution of the state $|1,n,z\rangle$ determined by the position dependent function $\phi_1(z,t)$, Eq. (25). As a consequence, the QAA should be a good approximation in this case. Nevertheless, it was also noted that the QAA cannot reproduce all the effects, for instance, the norm of $\phi_2(z,t)$ changes its value by more than 100% inside the cavity when using the exact quantum treatment while it would remain constant in the QAA. Note that using directly the states $\psi_{\pm n}(z,t)$ in the exact quantum treatment allows a straightforward reading of some properties as the atom transits the cavity, while the space dependence of the states $|j,n,z\rangle$ ($j = 1,2$) along with time and space dependence of $\phi_j(z,t)$ may make it less transparent.

C. Red detuning outside the transmission-resonance regime

The wave packets for red detuning $\psi_{\pm 0}(z,t)$ exhibit similar dynamics to the case of $\psi_{+0}(z,t)$ with zero detuning, especially

at the cold regime. In fact, in that regime and for sufficiently long times, the structure of all the wave packets is similar to that illustrated for the imaginary part of $\psi_{+0}(z,t)$ in Fig. 1(c), and the corresponding PPDF is essentially Gaussian. In the intermediate regime $\psi_{\pm 0}(z,t)$ are divided into transmitted and reflected wave packets for the velocities $v = 27$ and 43 cm/s very similarly to $\psi_{+0}(z,t)$ in Figs. 1(i) and 1(o). The reflected parts of both the wave packets and the corresponding position probability density functions resemble a train of quasi-Gaussian packets, i.e., they have an echolike structure very much like that shown in the mentioned figures.

Using the SCAA we find that the atom moves under the repulsive potential $E_{+0}(z)$ with an energy $E = (1/2)Mv^2 + E_{+0}(\mu)$, see Eqs. (19)–(24) and the definition of μ and v in Sec. IV. Therefore, we would expect that the atom should always be reflected as long as E is smaller than the maximum height $(\hbar/2)(\sqrt{\delta_L^2 + 4g_0^2} - |\delta_L|)$ of $E_{+0}(z)$. On the other hand, the atom should always be transmitted if E is larger than this height. For $\delta_L = -g_0/16$ the aforementioned maximum height of $E_{+0}(z)$ is equal to $0.97 * \hbar g_0$. Hence, the SCAA predicts that the atom will be reflected for the initial mean velocities $v = 3.9, 27$ cm/s and that the atom will be transmitted for the initial mean velocity $v = 43$ cm/s (see Sec. IV for the corresponding initial mean kinetic energies in terms of $\hbar g_0$). Our numerical simulations show that there is significant deviation with this behavior in the intermediate regime due to the quantum treatment of the center-of-mass motion for red detunings. For $\delta_L = -g_0/16$ and velocities $v = 3.9, 27$, and 43 cm/s, the atom has respective probabilities of 100, 96.4, and 30% of being reflected by the cavity field. The result for the largest velocity is specially different from that predicted by the SCAA. The difference with the SCAA and its breakdown is mainly due, as in the blue detuning case, to the large dispersion in position and momentum that results when the center-of-mass motion is quantized. Also, a source
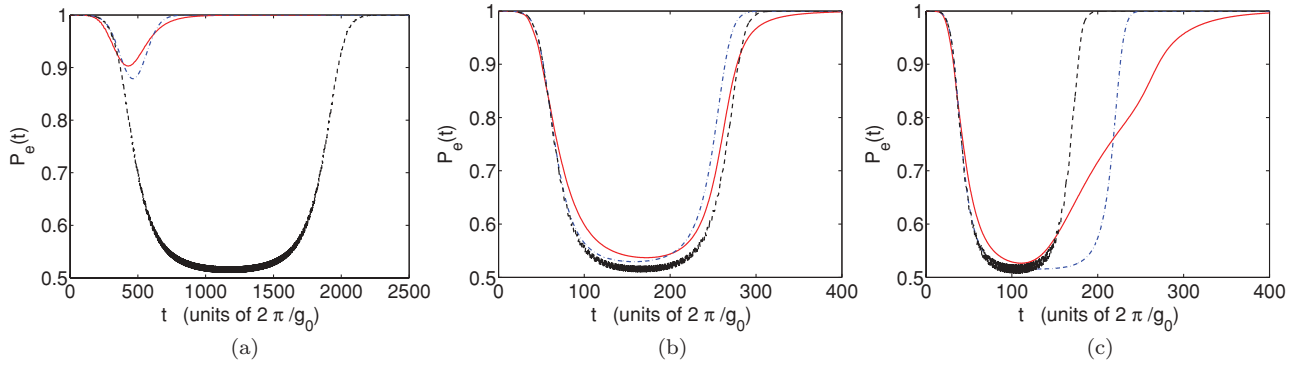
FIG. 8. (Color online) the probability of finding the atom in the excited state for red detuning, $\delta_L = -g_0/16$. Each part of the figure illustrates the result obtained when the center-of-mass motion is quantized (red solid line), treated in the semiclassical adiabatic approximation (blue dash-dot line), or, finally, follows the classical trajectory $z = vt + \mu$, where v is the initial velocity and μ the initial position (black dashed line). μ is equal to the initial mean position of the atom in the quantum treatment. Results are shown for initial velocities (a) $v = 3.9$ cm/s, (b) 27 cm/s, and (c) 43 cm/s. Time is in units of $2\pi/g_0$.

of differences with the SCAA for the $v = 27$ cm/s case is that $|\psi_{+0}(t)\rangle$ has large-enough kinetic energy to tunnel appreciably through the repulsive potential $V_n(\mathbf{R})$, although this statement should be taken with care because we are dealing with coupled differential equations, Eq. (28).

Asymptotically the semiclassical adiabatic approximation gives the correct value for the probability to find the atom in the excited state outside the transmission-resonance regime (Fig. 8). When the atom is in the interaction region the SCAA also gives a good qualitative (but not quantitative) approximation to the exact quantum treatment for the smallest velocities studied, which is not the case for the $z = vt + \mu$ treatment. The SCAA reproduces the inverted bell-like structure of $P_e(t)$ which takes on its minimum value approximately when the expected value of the position of the atom is near the center of the interaction region (Figs. 8 and 9). Also note that there is considerable difference between the SCAA and the exact quantum treatment in the structure of the probability to find

the atom in the excited state for the case of the highest velocity, since the reflection due to the width in momentum of the wave packet is much more relevant in this case.

In the exact quantum treatment the asymptotic behavior of the linear entropies and the entanglement of formation is easily understood using the same argument as in the blue detuning case, and the structure of $S_L^{\text{c.m.}}(t)$ when the atom is in the interaction region can be understood by observing Fig. 10(c).

As in the blue detuning case, if one uses the semiclassical adiabatic approximation, one expects that the system asymptotically has the atom in the excited state and the cavity-field with zero photons. Therefore, the system should be found asymptotically in a pure separable state. Although this does happen asymptotically in the exact quantum treatment, the SCAA is not strictly valid and cannot describe quantitatively what happens inside the interaction region, as illustrated in Fig. (10) for $\delta_L = -g_0/16$.
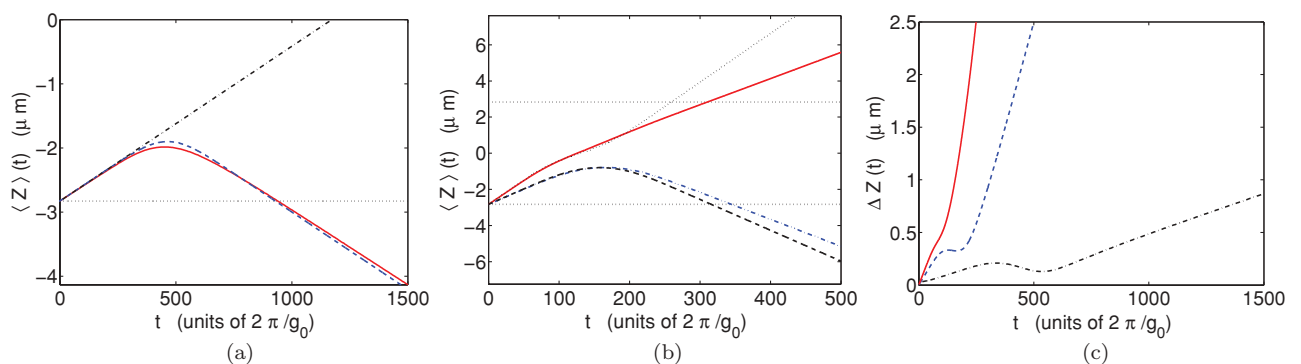
FIG. 9. (Color online) For red detuning, $\delta_L = -g_0/16$, (a) the expected value of the position of the atom when the initial velocity is $v = 3.9$ cm/s for a full quantum treatment (red solid line), for the SCAA (blue-dashed), and for the $z = vt + \mu$ treatment of the center-of-mass motion (black dash-dot line) (μ is equal to the initial mean position of the atom in the quantum treatment). (b) The expected values of the position of the atom with the initial velocity $v = 27$ cm/s for the full quantum treatment (blue dash-dot line) and for the SCAA (black dashed line). It also shows $\langle Z \rangle$ for the initial velocity 43 cm/s resulting from the full quantum treatment (red solid line) and for SCAA (black dotted line). The horizontal dotted lines indicate the limits of the interaction region. (c) The standard deviation of the position of the atom when the center-of-mass motion is quantized with the initial velocities $v = 3.9$ cm/s (black dash-dot line), 27 cm/s (blue dashed line), and 43 cm/s (red solid line). In all figures time is in units of $2\pi/g_0$.

D. Transmission-resonance regime

For $\delta_L \equiv \omega_L - \omega_A = 0$, stationary states of the model Hamiltonian (1) with very low energy with respect to the atom-field coupling energy $\hbar g_0$ exhibit resonances in some properties for certain values of the length L of the atom-field interaction region [5,21,28]. The precise conditions for the occurrence of these resonances depend greatly on the mode function $u(z)$ considered. Exact analytic expressions for the conditions necessary to have resonances in the probability of emission have been found for the mesa $u(z) = \theta(z)\theta(L - z)$ (θ is the Heaviside function) and $u(z) = \text{sech}^2(z/L)$ profiles [5], and they relate the de Broglie wavelength of the stationary state to L. The Gaussian mode has been treated numerically and the resonances for the probability of emission were studied for the particular value of the energy $E = \hbar g_0/100$ as a function of the waist w_0 of the Gaussian mode in Ref. [28]. In the cases we have treated in previous sections the aforementioned resonances and their effects have not been observed even though we studied the case when the initial mean kinetic energy was precisely $K_0 = \hbar g_0/100$. The reason for this is that we took a standard deviation of the Gaussian mode of $w_0/\sqrt{2} = 10^{-6}/\sqrt{2}$ m, and much smaller values of this quantity are needed in order to observe them at this energy, Ref. [28].

In this section we will study the properties of the CQED system at the transmission-resonance regime with fixed initial mean kinetic energy, $K_0 = \hbar g_0/100$, and initial standard deviation of position $\Delta = 10^{-8}$ m, w_0 variable, and the rest of the parameters as before. We have chosen these values for K_0 and Δ to compare and build on Refs. [21] and [28]. Note, however, that smaller values of K_0 and larger values of Δ can also yield transmission resonances; the main point is that resonances are observed for w_0 smaller than Δ, as realized in Ref. [21] when dealing with an initial Gaussian wave packet.

It is important to delve a bit more into the parameters we used in the numerical simulation in order to understand some of the results. Since we took $K_0 = \hbar g_0/100$ as the expected value of the kinetic energy of the atom at time $t = 0$, the initial mean momentum of the atom is $p_0 = 10\sqrt{2M\hbar g_0}$ with $M = 1.4 \times 10^{-25}$ kg as the mass of the atom. Therefore, the initial relative standard deviation in momentum is

$$\frac{\Delta_p}{p_0} = \frac{5}{\Delta}\sqrt{\frac{\hbar}{2Mg_0}} = 0.94, \tag{42}$$

because the standard deviation in position at time $t = 0$ was taken as $\Delta = 10^{-8}$ m and we are dealing with minimum uncertainty wave packets, Eqs. (31) and (32). Furthermore, the relative standard deviation in position was taken as

$$0.05 \leqslant \frac{\Delta}{|\mu|} \leqslant 3.5, \tag{43}$$

since the expected value of position at time $t = 0$ was taken as $\mu = -4w_0/\sqrt{2}$ and the waist w_0 of the Gaussian mode was varied from 10^{-9} m to 7×10^{-8} m. As a consequence, the wave packets at time $t = 0$ are not well localized in momentum, and they pass from not being well localized in position to being well localized in position as w_0 increases. As will be discussed below, the large relative standard deviation in momentum can lead to an attenuation of the resonances.

Figure 11(a) presents the probability $T(w_0)$ for the atom to be transmitted through the cavity field as a function of the Gaussian mode waist w_0 for the three values of the detuning considered above. The numerical simulation was stopped after a time $t_f = 21w_0\sqrt{M/K_0}$ which corresponds to three times the classical transit time of the interval $(-7w_0/\sqrt{2}, 7w_0/\sqrt{2})$ by a free atom with kinetic energy K_0. In the figure it can be observed that $T(w_0)$ differs dramatically from the results of previous sections. When there is zero detuning ($\delta_L = 0$) $T(w_0)$ is always less than 0.5 and oscillates with decreasing amplitude
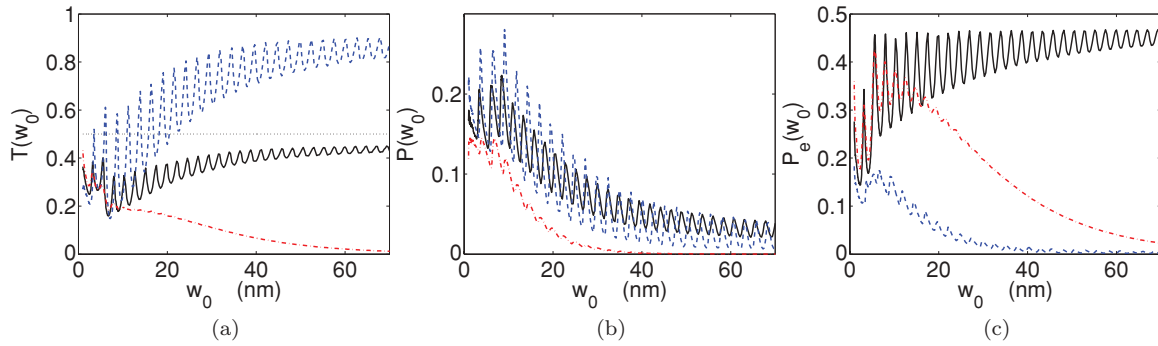
FIG. 11. (Color online) (a) The probability $T(w_0)$ that the atom is transmitted through the cavity field, (b) the probability of finding the atom inside the interaction region $(-4w_0/\sqrt{2}, 4w_0/\sqrt{2})$, and (c) the probability of emission (equal to 1 minus the probability of finding the atom in the excite state), all as a function of the Gaussian mode waist w_0 at time $t_f = 21w_0\sqrt{M/K_0}$ for the initial mean kinetic energy $K_0 = \hbar g_0/100$. Blue dashed lines correspond to a detuning $\delta_L = g_0/16 > 0$, black solid lines correspond to zero detuning, and red dashed-dotted lines correspond to a detuning $\delta_L = -g_0/16 < 0$. The waist w_0 is in nanometers.

as w_0 increases so there are certain values of w_0 where $T(w_0)$ shows maxima. These are the transmission resonances alluded to in the paragraphs above. The differences with previous sections are due to the fact that both the repulsive potential $V_n(\mathbf{R})$ associated with $|\psi_{+n}(t)\rangle$ and the attractive potential $-V_n(\mathbf{R})$ associated with $|\psi_{-n}(t)\rangle$ are very narrow, as measured by the waist w_0, in comparison to the width Δ of the wave packets. As a consequence of this, there is great tunneling by $|\psi_{+n}(t)\rangle$ and large reflection by $|\psi_{-n}(t)\rangle$. On the other hand, in previous sections the waist w_0 of the potential was much larger than the width Δ and, hence, the aforementioned tunneling and reflection were negligible for this initial mean kinetic energy. Taking a look at Figure 11(a), one can see that the resonances start to disappear and $T(w_0)$ slowly tends to the value of $1/2$ reported in previous sections as w_0 becomes larger than Δ.

When there is blue detuning ($\delta_L > 0$) the atom is reflected with greater probability when $w_0 \lesssim 2\Delta$, except at the values of w_0 where the aforementioned resonances occur. These are now slightly shifted and more pronounced in comparison to the case of zero detuning. Also note that $T(w_0)$ tends slowly to the value of 1 of previous sections. The case of red detuning ($\delta_L < 0$) shows that the atom has considerable probability to be transmitted through the cavity field, especially at the resonances that, although present, are now less pronounced and disappear very rapidly. Observe that $T(w_0)$ rapidly tends to the stationary value of 0 of previous sections as w_0 becomes larger than Δ. The behavior of $T(w_0)$ indicates a complete breakdown of the semiclassical adiabatic approximation, since it predicts that the atom will always be transmitted for blue detuning and always be reflected for red detuning. The reason for this is that now the quantum effects of tunneling and reflection mentioned in the previous paragraph in the coupled equations (28) are very large.

The results for the probability $T(w_0)$ of the atom to be transmitted through the cavity field as a function of the Gaussian mode waist w_0 in the cases of zero and red detunings can be compared with those of Ref. [21]. Our results agree with the structure of $T(w_0)$ presented in that reference but differ quantitatively in the case of zero detuning. Reference [21] presents resonances that do reach the value of $1/2$ and $T(w_0)$ reaches the stationary value of $1/2$ more rapidly. The reason for this difference is explained in the following paragraph.

Figure 11(b) illustrates the probability to find the atom inside the interaction region $(-4w_0/\sqrt{2}, 4w_0/\sqrt{2})$ at time $t_f = 21w_0\sqrt{M/K_0}$. It is interesting that this trapping probability is not negligible for long times such as t_f, although it tends to zero as w_0 increases. This effect partially accounts for $T(w_0)$ not reaching a value of $1/2$ at the transmission resonances. The other factor, which is also related to this non-negligible trapping probability, resides in the different initial conditions used in Ref. [21]. Of particular importance is the relative standard deviation in momentum, since our wave packets are not well localized in momentum [see Eq. (43)] and the wave packets taken in Ref. [21] have $\Delta_p/p_0 = 1/3$ with Δ_p the standard deviation in momentum and p_0 the mean momentum, both at time $t = 0$. Therefore, a large relative standard deviation in momentum can lead to an attenuation of the transmission resonances. A similar effect was found in Ref. [21], were it was realized that larger widths in momentum tend to attenuate and smear out variations and resonances for $T(w_0)$ in the mesa function and sech^2 function profiles for zero detuning interactions.

Figure 11(c) illustrates the probability of emission $P_{em}(w_0) = 1 - P_e(w_0)$. Resonances are clearly marked for the zero detuning case ($\delta_L = 0$) and they are still present, although not so pronounced, for blue detuning ($\delta_L > 0$). The red detuning case ($\delta_L < 0$) has marked resonances when w_0 is smaller than Δ, but they rapidly disappear as Δ becomes larger than w_0. The differences with the results of the previous sections can be understood by taking a look at Eq. (9). In the regime that we are now discussing, the real part of the overlap $\langle\psi_{+n}(t)|\psi_{-n}(t)\rangle$ is now large, since, as discussed above, $|\psi_{-n}(t)\rangle$ is considerably reflected and $|\psi_{+n}(t)\rangle$ is considerably transmitted. Finally, note that for all values of the studied detunings $P_e(w_0)$ slowly tends to the corresponding values of previous sections as w_0 becomes larger than Δ.

These results using an initial minimum-uncertainty wave packet to describe the center-of-mass motion can be compared with those using stationary states with defined energy to describe the system. In Ref. [28] the probability of emission is reported for a Gaussian profile, stationary states with energy K_0, and values of w_0 that correspond to the region between 0 and 43 (nm) in our setup. For these stationary states the resonances in the probability of emission always reach a
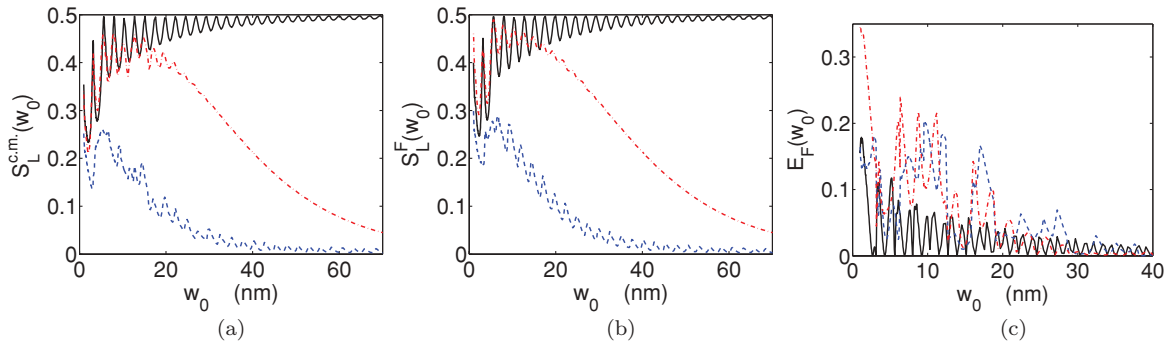
FIG. 12. (Color online) [(a), (b), and (c)] Respectively, the linear entropy of the center-of-mass density operator, the linear entropy of the field density operator, and the entanglement of formation of the density operator of the internal atom and field degrees of freedom as a function of the Gaussian mode waist w_0 at time $t_f = 21 w_0 \sqrt{M/K_0}$ for the initial mean kinetic energy $K_0 = \hbar g_0/100$. The linear entropy of the internal atom degrees of freedom is the same as in (b) [see Eq. (12) and the paragraph below it]. In the interval from 40 to 70 nm, the entanglement of formation for all values of the detuning decreases to zero (not shown for purposes of better illustration in the region presented). Blue dashed lines correspond to a detuning where $\delta_L = g_0/16$, black solid lines correspond to zero detuning, and red dashed-dotted lines correspond to a detuning where $\delta_L = -g_0/16$. The waist w_0 is in nanometers.

maximum value of 1/2, decrease in amplitude as the w_0 increases, and nearly acquire the stationary value of 1/2 when $w_0 = 43$ (nm). Our results show that for Gaussian wave packets such as ours the probability of emission is always less than 1/2 and tends to the stationary value of 1/2 much more slowly. Similarly to $T(w_0)$, this difference can be due to position and momentum widths of the initial wave packet [see Eqs. (42) and (43)], which can be expressed as a superposition of stationary states that in general would not all be resonant at the same w_0 of the Gaussian profile. The effect of the widths is present in the probability of emission by means of the overlap $\langle \psi_{+n}(t)|\psi_{-n}(t)\rangle$, Eq. (9).

Figures 12(a) and 12(b) present the linear entropies of the density operators of the center-of-mass and field degrees of freedom as a function of w_0, respectively (remember that the linear entropy of the density operator of the internal atom degrees of freedom is the same as that of the field degrees of freedom). Since these quantities depend greatly on the overlap $\langle \psi_{+n}(t)|\psi_{-n}(t)\rangle$ and on the probability to find the atom in the excited state [see Eqs. (11) and (12)], they can be highly affected by the now relevant quantum effects of tunneling and reflection explained above. When there is zero detuning ($\delta_L = 0$) resonant effects are sharply marked and the reduced state tends to a maximum mixed state as w_0 becomes larger. When there is red detuning ($\delta_L < 0$) the oscillatory behavior of the linear entropies is less pronounced and disappears rapidly for increasing w_0. In this case the reduced states first tend to maximum mixed states and finally asymptotically approach pure states as w_0 becomes larger. The case of blue detuning ($\delta_L > 0$) exhibits a smaller oscillatory behavior that persists for higher values of w_0, a result that is in accordance with the behavior exhibited by $P_{em}(w_0)$ [Fig. 11(c)]. Also, for blue detuning the linear entropies tend to zero as w_0 increases. Hence, the results of previous sections are recovered for the three values of the detuning presented as w_0 becomes larger than the width Δ of the wave packets.

Figure 12(c) shows the entanglement of formation E_F between the internal atom and field degrees of freedom as a

function of w_0. This quantity is also determined by $P_e(w_0)$ and the overlap $\langle \psi_{+n}(t)|\psi_{-n}(t)\rangle$ as can be seen in Eqs. (13)–(17). It can be observed that E_F has a complex structure and is zero just for a discrete set of w_0. Therefore, the internal atom and field degrees of freedom are entangled for the three values of the detuning considered. This situation contrasts greatly with the results of previous sections, since it was found that these degrees of freedom were not entangled asymptotically for the three values of the detuning. Other consequences of these new results in this transmission-resonance regime is that the system does not exhibit genuine tripartite entanglement for the zero detuning case and the system is not in a product state when detuning differs from zero. Nevertheless, note that the results of the previous sections are again recovered as w_0 becomes larger than the width Δ of the wave packets.

VI. CONCLUSIONS

In this article we studied the temporal evolution of a two-level atom with its center-of-mass motion quantized in one dimension and interacting with a single-mode quantum cavity field with a Gaussian profile. The initial internal state was taken to be the excited atomic state with no photons inside the cavity, while the initial center-of-mass state was described by a minimum-uncertainty Gaussian wave packet. As a consequence, the natural basis describes the particle as a superposition of the wave packets $\psi_{\pm n}(z,t)$.

In the first part, the center-of-mass motion of the atom had an initial standard deviation of position much smaller than the waist of the Gaussian cavity field, and hence the system was outside the transmission-resonance regime. The analysis was performed for various values of the detuning between the atomic transition and the cavity-field frequencies and for various values of the initial mean velocities of the matter waves. The wave packets $\psi_{\pm n}(z,t)$ and the corresponding position probability density functions evolve so that asymptotically they may preserve Gaussian structures or exhibit precursors and echolike forms. It was explicitly shown

that, in the cold and intermediate regimes, the probability of emission and the entanglement present in the system differ greatly to the case where the center-of-mass motion is treated as $z = vt + \mu$ or within the semiclassical adiabatic approximation.

In the case of zero detuning and outside the transmission-resonance regime, we observed that in the cold regime the probability of emission does not exhibit the well-known Rabi oscillations is always less than 1 and takes on the final value of 1/2 once the atom leaves the interaction region. The onset of Rabi-like oscillations was also observed for a high-enough initial mean kinetic energy. It was also shown that in the cold and intermediate regimes, the system as a whole presents genuine tripartite entanglement, a totally different behavior from the classical case because the internal atom degrees of freedom and the field are in a maximum mixed separable state. Note that unlike GHZ states, in this case tripartite entanglement involves discrete and continuous degrees of freedom.

In the case of detuning on the order of g_0 and outside of the transmission-resonance regime, our exact treatment showed that for blue detuning the atom is always transmitted through the cavity field, while in the case of red detuning the atom can still be reflected considerably even when its initial kinetic energy is slightly larger than the atom-field coupling energy. In both cases the atom leaves the cavity in the excited state, and the whole system is in a product state such that $|\psi_{+n}(t)\rangle = |\psi_{-n}(t)\rangle$. It is noteworthy that the temporal evolution of $\psi_{\pm n}(z,t)$ in the case of blue detuning showed that $\psi_{+n}(z,t)$ almost disappears completely when the atom is found with almost certainty inside the interaction region and later reappears once the atom has left it. In spite of this the semiclassic adiabatic approximation gives the correct result for the asymptotic values of various properties of the system, except for transmission probabilities in the case where there is red detuning and the initial mean kinetic energy of the atom is slightly higher than the atom-field coupling energy.

In the second part of this article we studied the properties of the system in the so-called transmission-resonance regime. For the initial state considered with a small-enough initial mean kinetic energy, the relation between the following two parameters determine if the system is in this regime: the waist w_0 of the Gaussian mode and the width Δ of the initial Gaussian wave packets describing the center-of-mass motion. If w_0 is smaller or comparable to Δ, then the system is in the aforementioned regime (for a small-enough initial mean kinetic energy) and many properties take values that differ greatly from those presented in the first part of the article. Our results show how these quantities recover the corresponding values of the first part as w_0 increases and becomes larger than Δ. The origin of the differences lies in the overlap $\langle\psi_{+n}(t)|\psi_{-n}(t)\rangle$, since most properties of the system depend on it and its value depends on how w_0 is compared to Δ.

While this overlap may be zero when w_0 is much larger than Δ, this is not the case by far when $w_0 \lesssim \Delta$. In the latter case quantum effects of tunneling and reflection respectively by effective repulsive and attractive potentials become dominant. It is noteworthy that for long times there is a non-neglibible probability of finding the atom in the interaction region, a property that disappears as w_0 gradually becomes larger than Δ. It is also very important to note that a large relative standard deviation in momentum can lead to a considerable attenuation of the resonances for the probability of transmission through the cavity field and the probability of emission for all values of the detuning.

It was also found that many properties are greatly affected by the detuning δ_L between the cavity-field frequency and the atomic transition frequency. When $\delta_L \neq 0$, the oscillations tend to be less pronounced and disappear more rapidly when compared to the case where $\delta_L = 0$, especially for the case where $\delta_L < 0$. This behavior was found for all properties of the system, except for the probability of being transmitted through the cavity field in the case of $\delta_L > 0$ and for the entanglement of formation for $\delta_L \neq 0$. The former exhibits sharper oscillations with greater amplitude and the latter exhibits wilder oscillations. The dependence of the von Neumann entropy and the probability of being transmitted through the cavity field on the detuning had already been presented for the case where $\delta_L < 0$ in Ref. [21] and the results of that article agree with ours.

In the transmission-resonance regime, the entanglement and degree of mixedness are greatly affected for all values of the detuning. There is no genuine tripartite entanglement for $\delta_L = 0$ in this regime except for a discrete number of values of w_0, and the system is no longer asymptotically in a product state for $\delta_L \neq 0$. This is due to the fact that the internal atom and field degrees of freedom are now entangled for all values of the detuning. Furthermore, all bipartite reductions of the state of the system are now no longer maximally mixed. It is important to emphasize that the genuine tripartite entanglement for $\delta_L = 0$ and the product states for $\delta_L \neq 0$ are recovered as w_0 increases and becomes larger than Δ.

We expect the results reported in this article to be qualitatively valid also for other field modes that have a Gaussian-like structure such as the sech^2 function. This is not the case for potentials that have discontinuities such as the mesa profile, since it has already been realized that the discontinuities are a source of very different dynamics [21]. Also, a very important factor that needs analysis is dissipation, which may alter greatly the evolution of the center-of-mass motion [2] unless proper values of the atom-field couplings are achieved.

[1] B.-G. Englert, J. Schwinger, A. O. Barut, and M. O. Scully, Europhys. Lett. **14**, 25 (1991).

[2] M. Battocletti and B.-G. Englert, J. Phys. II (France) **4**, 1939 (1994).

[3] M. O. Scully, G. M. Meyer, and H. Walther, Phys. Rev. Lett. **76**, 4144 (1996).

[4] G. M. Meyer, M. O. Scully, and H. Walther, Phys. Rev. A **56**, 4142 (1997).

[5] M. Löffler, G. M. Meyer, M. Schröder, M. O. Scully, and H. Walther, Phys. Rev. A **56**, 4153 (1997).

[6] M. Schröder, K. Vogel, W. P. Schleich, M. O. Scully, and H. Walther, Phys. Rev. A **56**, 4164 (1997).

[7] C. J. Hood, T. W. Lynn, A. C. Doherty, A. S. Parkins, and H. J. Kimble, Science **287**, 1447 (2000).

[8] T. Bastin and J. Martin, Phys. Rev. A **67**, 053804 (2003).

[9] T. Bastin and J. Martin, Phys. Rev. A **72**, 053815 (2005).

[10] J. Martin and T. Bastin, Eur. Phys. J. D **48**, 301 (2008).

[11] F. Brennecke, T. Donner, S. Ritter, T. Bourdel, M. Köhn, and T. Esslinger, Nature (London) **450**, 269 (2007).

[12] Y. Colombe, T. Steinmetz, G. Dubois, F. Linke, D. Hunger, and J. Reichel, Nature (London) **450**, 272 (2007).

[13] S. Gupta, K. L. Moore, K. W. Murch, and D. M. Stamper-Kurn, Phys. Rev. Lett. **99**, 213601 (2007).

[14] R. Juárez-Amaro, J. M. Vargas-Martínez, and H. Moya-Cessa, Laser Phys. **18**, 344 (2008).

[15] C. Cohen-Tannoudji, J. Dupont-Roc, and G. Grynberg, *Atom-Photon Interactions: Basic Processes and Applications* (Wiley, New York, 1998).

[16] S. Haroche, M. Brune, and J. M. Raimond, Europhys. Lett. **14**, 19 (1991).

[17] S. Haroche and J. M. Raimond, in *Advances in Atomic, Molecular and Optical Physics, Supplement 2*, edited by P. R. Berman (Academic Press, New York, 1994), pp. 123–170.

[18] J. Larson and S. Stenholm, Phys. Rev. A **73**, 033805 (2006).

[19] S. V. Prants, M. Yu. Uleysky, and V. Yu Argonov, Phys. Rev. A **73**, 023807 (2006).

[20] J. Larson and M. Abdel-Aty, Phys. Rev. A **80**, 053609 (2009).

[21] J. Larson, J. Phys. B: At. Mol. Opt. Phys. **42**, 044015 (2009).

[22] J. M. Raimond, M. Brune, and S. Haroche, Rev. Mod. Phys. **73**, 565 (2001).

[23] M. Plenio and S. Virmani, Quantum Inf. Comput. **7**, 1 (2007).

[24] W. E. Schiesser, *The Numerical Method of Lines: Integration of Partial Differential Equations* (Academic Press, San Diego, 1991).

[25] W. E. Schiesser and G. W. Griffiths, *A Compendium of Partial Differential Equation Models: Method of Lines Analysis with Matlab* (Cambridge, New York, 2009).

[26] K. W. Morton and D. F. Mayers, *Numerical Solution of Partial Differential Equations*, 2nd ed. (Cambridge, UK, 2005).

[27] D. F. Walnut, *An Introduction to Wavelet Analysis* (Birkhäuser, Boston, 2001).

[28] T. Bastin and E. Solano, Comput. Phys. Commun. **124**, 197 (2000).

[29] P. Münstermann, T. Fischer, P. Maunz, P. W. H. Pinkse, and G. Rempe, Phys. Rev. Lett. **82**, 3791 (1999).

[30] R. W. Boyd and D. J. Gauthier, in *Progress in Optics*, edited by E. Wolf (Elsevier, Amsterdam, 2002), Vol. 43, pp. 497–530.

[31] Two computer movies of the time evolution labeled by the authors' names can be downloaded from [www.fisica.unam.mx/research/movies].

[32] R. Horodecki, P. Hodorecki, M. Hodorecki, and K. Hodorecki, Rev. Mod. Phys. **81**, 865 (2009).